JACS
JOURNAL OF THE AMERICAN CHEMICAL SOCIETY

Article

pubs.acs.org/JACS

Hierarchical Self-Assembly of Polyoxometalate-Based Hybrids Driven by Metal Coordination and Electrostatic Interactions: From Discrete Supramolecular Species to Dense Monodisperse Nanoparticles

Guillaume Izzet,[*,§] Benjamin Abécassis,[†] Dalil Brouri,[‡] Madeleine Piot,[§] Benjamin Matt,[§] Stefano Artin Serapian,[∥] Carles Bo,[∥,⊥] and Anna Proust[§]

[§]Sorbonne Universités, UPMC Université Paris 06, CNRS UMR 8232, Institut Parisien de Chimie Moléculaire, Université Pierre et Marie Curie, 4 Place Jussieu, F-75005 Paris, France

[†]Laboratoire de Physique des Solides, Université Paris-Sud, CNRS UMR 8502, 91405 Cedex Orsay, France

[‡]Sorbonne Universités, UPMC Université Paris 06, CNRS UMR 7197, Laboratoire de Réactivité de Surface, Université Pierre et Marie Curie, 4 Place Jussieu, F-75005 Paris, France

[∥]Catalan Institute of Chemical Research (ICIQ), The Barcelona Institute of Science and Technology, Avinguda dels Països Catalans 16, 43007 Tarragona, Spain

[⊥]Departament de Química Física i Inorgànica, Universitat Rovira i Virgili, Avinguda dels Països Catalans, 26, 43007 Tarragona, Spain

Supporting Information

ABSTRACT: The metal-driven self-assembly processes of a covalent polyoxometalate (POM)-based hybrid bearing remote terpyridine binding sites have been investigated. In a strongly dissociating solvent, a discrete metallomacrocycle, described as a molecular triangle, is formed and characterized by 2D diffusion NMR spectroscopy (DOSY), small-angle X-ray scattering (SAXS), and molecular modeling. In a less dissociating solvent, the primary supramolecular structure, combining negatively charged POMs and cationic metal linkers, further self-assemble through intermolecular electrostatic interactions in a reversible process. The resulting hierarchical assemblies are dense monodisperse nanoparticles composed of ca. 50 POMs that were characterized by SAXS and transmission electron microscopy (TEM). This multiscale organized system directed by metal coordination and electrostatic interactions constitutes a promising step for the future design of POM self-assemblies with controllable structure-directing factors.

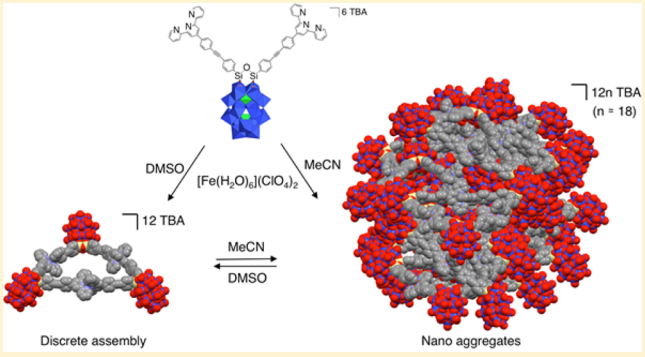

INTRODUCTION

The control of molecular organization from small molecular building blocks by self-assembly is a major challenge in supramolecular chemistry.[1] The design of nanoscale materials with hierarchical order and complexity opens up important perspectives for a wide range of technological applications.[2−5] In this context, the elaboration of functional materials integrating polyoxometalates (POMs) as molecular building blocks is particularly attractive owing to their various properties and potential applications.[6−8] POMs are anionic nanosized molecular metal−oxides that bridge the gap between small oxo−metal complexes and bulk metal−oxides. Nanostructured assemblies containing POMs have been mostly developed from POM-based surfactant hybrids.[9,10] In such systems, the POM is associated with amphiphilic moieties either through electrostatic interaction or by a covalent anchorage. The formation of highly ordered films,[11] liquid crystals phases,[12−14] hollow spheres,[15−17] micelles,[18] microemulsion[19] or smart photo-responsive systems[20] through self-assembly processes of POMs has thus been described. Metal-directed self-assembly is also a powerful tool for the synthesis of discrete 0D to extended 3D assemblies.[21,22] As regards POM chemistry, a plethora of POM-based coordination polymers have been obtained through reactions of POMs with organic ligands and metal salts, most often under hydrothermal conditions.[23,24] While this method has proven successful in the production of crystalline open-framework materials with 3D topologies, it does not afford much control of dimensionality. In contrast, metal driven self-assembly of preformed covalent POM hybrids bearing remote binding sites has been very scarcely described in the literature, while this approach is well-suited for the rational design of organized nanoarchitectures.[25−29]

Received: January 27, 2016
Published: March 28, 2016

DOI: 10.1021/jacs.6b00972
J. Am. Chem. Soc. 2016, 138, 5093−5099

Scheme 1. Synthetic Route to the D_{Si}[tpy] Hybrid[a]

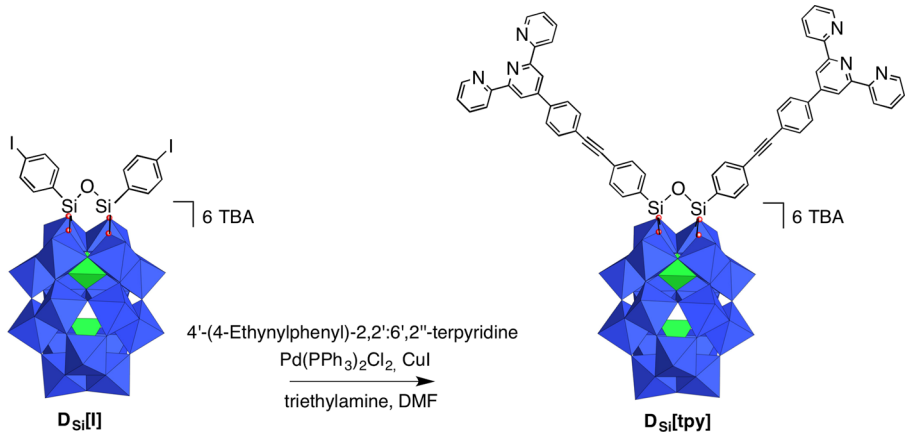

[a]In the polyhedral representation, the WO_6 octahedra are depicted with oxygen atoms at the vertices and metal cations buried inside. Color code: WO_6 octahedra, blue; PO_4 tetrahedra, green.

Our expertise in the field of covalent POM-based hybrids drove us to elaborate controllable POM-based nanoarchitectures through metal directed self-assembly. We recently described a covalent POM-based molecular triangle and characterized it through a combination of complementary analytical techniques (DOSY NMR, SAXS, and TWIM MS) that proved to be relevant tools for probing the chemical structure of such large assemblies.[30] The system developed was obtained through the reaction between an organosilyl functionalized Dawson-type POM displaying two terminated-pyridine binding sites and one equivalent of a linear neutral metal linker, *i.e.*, *trans*-$[PdCl_2(CH_3CN)_2]$. We herein explore the metal driven self-assembly of the bis-terpyridine analogue, in the presence of a cationic metal linker. In such a system, the combination of negatively charged POMs and cationic metal linkers favors the aggregation of the primary self-assembled structures into larger multiscale assemblies through intermolecular electrostatic interactions.[31−35] We also report that the aggregation of the primary supramolecular structures is controlled by the nature of the solvent.

RESULTS AND DISCUSSION

Synthesis of the POM-Based Molecular Platform. The POM-based building block $[P_2W_{17}O_{61}\{O(Si{-}C_{29}H_{18}N_3)_2\}]^{6-}$ denoted $\mathbf{D_{Si}[tpy]}$[36] contains two terpyridine (tpy) units connected to the monolacunary site of a Dawson-type α_2-$[P_2W_{17}O_{61}]^{10-}$ through a Si−O−Si anchorage. Its synthesis is performed in one step from the iodo-aryl terminated POM-based platform $\mathbf{D_{Si}[I]}$ by adapting to our previously reported procedure involving a Sonogashira cross-coupling reaction (Scheme 1).[37] The hybrid $\mathbf{D_{Si}[tpy]}$ is isolated as a tetrabutyl ammonium (TBA) salt in good yield and characterized by ^{1}H and ^{31}P NMR spectroscopies, mass spectrometry, elemental analyses, and FT-IR spectroscopy (see Supporting Information (SI)).

Formation of a Discrete Molecular Triangle. Terpyridine ligands produce a linear arrangement when coordinated to an octahedral metal center such as Fe^{II}. The addition of $[Fe(H_2O)_6](ClO_4)_2$ to a colorless solution of $\mathbf{D_{Si}[tpy]}$ (1 mM) in DMSO instantly produces the characteristic purple color of the low spin Fe(II) bis-terpyridine complexes. ^{1}H NMR monitoring of the progressive addition of $[Fe(H_2O)_6](ClO_4)_2$ to a solution of $\mathbf{D_{Si}[tpy]}$ (1 mM in DMSO-d_6) shows the progressive formation of a new species displaying the same number of signals in the aromatic region and the concomitant disappearance of $\mathbf{D_{Si}[tpy]}$ (Figure 1). The reaction is total after the addition of 1 equiv of Fe per POM, in agreement with the formation of a supramolecular species displaying a 1:1 stoichiometry between the POM and the metal linker.

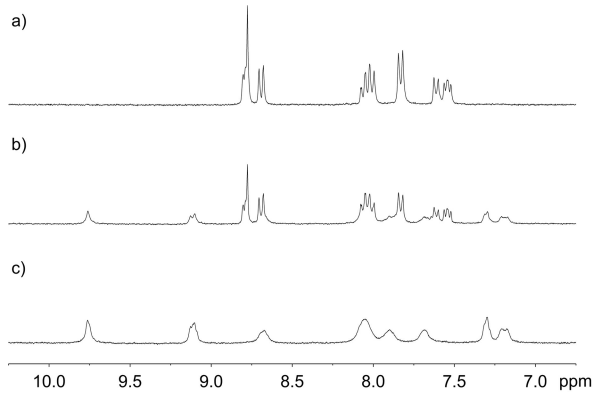

Figure 1. ^{1}H NMR (300 MHz, aromatic region) monitoring of the progressive addition of $[Fe(H_2O)_6](ClO_4)_2$ to a 1 mM solution of $\mathbf{D_{Si}[tpy]}$ in DMSO-d_6. (a) Before addition; (b) 0.5 equiv; (c) 1.0 equiv.

The ^{1}H NMR signals of the resulting supramolecular species are significantly broader than those of the parent hybrid $\mathbf{D_{Si}[tpy]}$. This is interpreted as the formation of larger species since the NMR signal line width is determined by T_2 relaxation, which is attenuated in large structures. The addition of an excess of diethyl ether to a solution containing $\mathbf{D_{Si}[tpy]}$ and 1 equiv of $[Fe(H_2O)_6](ClO_4)_2$ in DMSO leads to the precipitation of a purple solid. The infrared spectrum of the solid shows the absence of perchlorate, while the relative intensity of the signal corresponding the TBA cations are slightly attenuated (Figure S2). This suggests that upon the precipitation of the solid, the perchlorate ions remain in solution as TBA salt. Finally, upon dissolution of the purple solid in DMSO-d_6, the ^{1}H NMR signals of the resulting solution in the aromatic region match (without broadening) those of the solution prior to precipitation, suggesting that

DOI: 10.1021/jacs.6b00972
J. Am. Chem. Soc. 2016, 138, 5093−5099

perchlorate ions are not associated with the metallomacrocyle (Figure S3).

Diffusion-ordered NMR spectroscopy (DOSY) gives access to the translational diffusion coefficient, which is related to the size of the molecular assembly.[38,39] DOSY NMR experiments were performed on a 1 mM solution of $\mathbf{D_{Si}[tpy]}$ in DMSO-d_6 before and after the addition of 1 equiv of $[Fe(H_2O)_6](ClO_4)_2$ at T = 300 K. All aromatic signals of the resulting surpramolecular assembly give a unique diffusion coefficient, significantly lower than that of the parent hybrid (Figures S4 and S5, $D(\mathbf{D_{Si}[tpy]}) = 8.0 \times 10^{-11}$ m^2·s^{-1}, $D([(\mathbf{D_{Si}[tpy]}\cdot\mathbf{Fe}]) = 2.9 \times 10^{-11}$ m^2·s^{-1}). This suggests that all aromatic signals arise from species of similar shape and size, which precludes the formation of linear oligomeric species. The calculated hydrodynamic radius of a spherical particle with $D = 2.9 \times 10^{-11}$ m^2·s^{-1} (considering T = 300 K and η = 2.18 mPa·s[40]) is r_H = 3.5 nm according to the Stokes−Einstein equation. In the previously reported system based on a bis-pyridine analogue, the metal driven self-assembly led to a molecular triangle that was unambiguously characterized.[30] Owing to the structural similarity between both POM building blocks, it is likely that the supramolecular assemblies here characterized by DOSY NMR consist of molecular triangles.

To gain further insight into the structure of the cyclic oligomer, we seek to obtain the optimized structure of the molecular triangle, using density functional theory (DFT) as implemented by the program *ADF* (see SI for more details).[41,42] Its sheer size, characterized by 6804 electrons, constitutes a considerable computational challenge: it was therefore decided to start tackling the problem by breaking the system down into better-manageable fragments. We thus begin by performing separate preliminary optimizations of smaller species: a free unit of $\mathbf{D_{Si}[tpy]}$ as depicted in Scheme 1, and a "naked" (Dawson-free) triangle with neutral $[H_2C-O-CH_2]$ vertices replacing the formal $[O_2Si-O-SiO_2]^{4-}$, and Zn^{2+} replacing Fe^{2+}.

Both of these initial optimizations are performed using the BP86 density functional, featuring the exchange functional developed by Becke,[43] in conjunction with the P86 correlation functional developed by Perdew;[44,45] we also apply the D3 dispersion correction by Grimme[46] in combination with Becke−Johnson damping (D3(BJ)).[47,48] Electrons on all elements are modeled using a triple-ζ Slater-type basis set with one polarization function (TZP); core electrons are kept frozen, and treated with an appropriate relativistic frozen-core potential. Relativistic effects are introduced by means of the *zeroth-order regular approximation* (ZORA) in its scalar-relativistic form.[49,50] Electron integrals are numerically evaluated using Becke's integration grid[51] (quality: good).[52] Furthermore, at each step of the optimization, self-consistent field equations are solved using the nonstandard *indirect linear-expansion shooting technique* (LISTi):[53] this choice is found to be extremely useful in overcoming convergence issues. To better reflect experimental conditions, effects of DMSO are implicitly accounted for using the *conductor-like screening model* (COSMO) by Klamt et al.;[54−57] evaluation of the solvent cavity is performed by using the set of elemental radii purposely developed in 1998.[57] Finally, we note that the naked triangle is treated, with the D_3 symmetry point group.

Next, full molecular triangles are constructed by removing the $[H_2C-O-CH_2]$ vertices from the optimized "naked" structure, and replacing each of them with the $[P_2W_{17}O_{61}(OSi_2)]^{6-}$ part of the optimized $\mathbf{D_{Si}[tpy]}$ (i.e., omitting tpy units beyond the Si−C_{Ar} bond); Si−O−Si units are roughly positioned on the former coordinates of C−O−C vertices. The orientation of Dawson anions with respect to the plane of the molecular triangle gives rise to two possible isomers. With the aid of single-point energy calculations, conducted at the same level of theory described in the previous paragraph, we find that the lowest-energy isomer of the triangle is the one in which one of the POMs is angled away from the plane in the opposite direction compared to the other two (Figure 2), as found for the previously reported bis-pyridine polyoxometalate-based molecular triangle.[30]

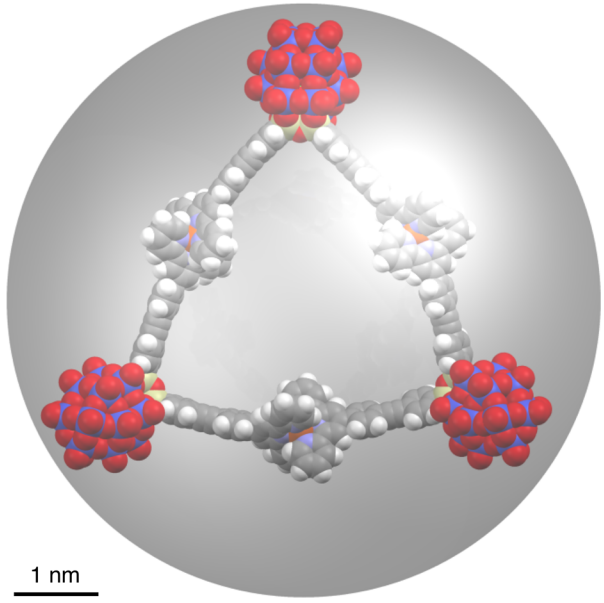

Figure 2. Comparison of the energy-minimized structure of the molecular triangle Zn^{2+}-analogue $[(\mathbf{D_{Si}[tpy]})_3\cdot\mathbf{Zn_3}]$ with a 3.5 nm radius sphere.

We finally proceed to optimize the lowest-energy isomer of the triangle using a special two-level treatment. For the Dawson anions, Si−O−Si units and adjacent phenyl rings, Zn^{2+} cations, and chelating N atoms in the tpy unit, we apply the same treatment used in the preliminary optimizations and single-point calculations. On the other hand, remaining regions are conveniently treated at a lower level of theory, which crucially allows to reduce computational time: the TZP basis set is thus replaced by a double-ζ counterpart, with no polarization functions (DZ); in addition, a coarser version of Becke's grid is used for evaluating electronic integrals (quality: normal).[51,52]

Coordinates of the optimized molecular triangle are provided in Table S1 and are also available online.[58] The tendency of each Si unit to preserve its tetrahedral structure, with O−Si−O angles of ∼109°, combined with the fact that the $[O_4]$ lacunae in Dawson anions cannot be distorted from their rectangular shape, lead to a certain amount of strain in the supramolecular structure: this translates into the organic moieties adopting a slight curvature, at the expense of some loss in aromaticity, and the Dawson moieties ending up slightly closer than expected. Such distortion is indeed confirmed by alternatively optimizing the triangle with the hybrid method *ONIOM*,[59] as implemented by the *Gaussian09* software package:[60] further details for this accessory optimization are given as SI, and coordinates are reported in Table S2 and are available online.[58]

DOI: 10.1021/jacs.6b00972
J. Am. Chem. Soc. 2016, 138, 5093−5099

On the other hand, we note that in the optimized $\mathbf{D_{Si}[tpy]}$ alone, where the organic tpy units are "open" and there is no source of strain, organic linkers remain straight. The energy-optimized structure of the molecular triangle has a radius of ca. 3.3 nm that is close to the calculated hydrodynamic radius r_H = 3.5 nm deduced from DOSY experiments. The modelization of a molecular triangle by a sphere particle is very simplistic since it does not account for its anisotropic and hollow shape and it neither considers the contribution of the solvent and the TBA to the translation diffusion of the overall assembly. However, as for the previous supramolecular triangle,[30] this model is fairly consistent with the computational optimized structure.

To complete the characterization of the cyclic supramolecular assembly, we performed SAXS (Small-Angle X-ray Scattering) experiments on dispersion of $\mathbf{D_{Si}[tpy]}$ in DMSO-d_6 before and after the addition of 1 equiv of $[Fe(H_2O)_6](ClO_4)_2$. SAXS is known to give insightful structural information on objects with sizes ranging from 1 to 100 nm.[61,62] We and others have successfully used SAXS to characterize POM-based supramolecular assemblies.[30,63−65] Figure 3a shows the SAXS

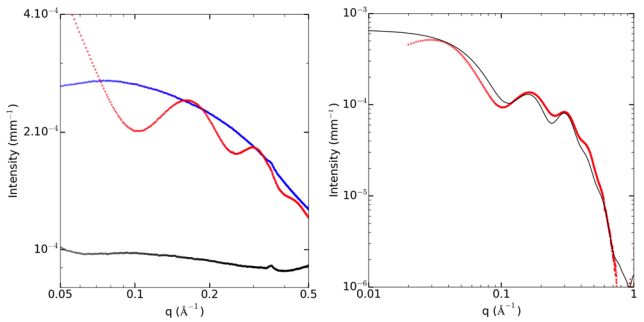

Figure 3. (Left) SAXS pattern of the solvent (DMSO-d_6, black), a solution of the molecular building-block $\mathbf{D_{Si}[tpy]}$ (1 mM in DMSO-d_6, blue) and the resulting molecular triangle $[(\mathbf{D_{Si}[tpy]})_3{\cdot}\mathbf{Fe_3}]$ (red). (Right) Comparison of the experimental SAXS pattern of $[(\mathbf{D_{Si}[tpy]})_3{\cdot}\mathbf{Fe_3}]$ (red) to the theoretical SAXS intensity (computed using CRYSOL) of the optimized structure (black).

pattern for the solvent, a solution of the molecular building-block $\mathbf{D_{Si}[tpy]}$ (1 mM in DMSO-d_6) and the resulting cyclic assembly. These SAXS patterns are very similar to those obtained in the previous bis-pyridine POM-based system. While the solvent pattern is almost flat, a significant SAXS signal is visible for the molecular building-block $\mathbf{D_{Si}[tpy]}$, consistent with well-dispersed nanometric objects. The small decrease in intensity at small wave vectors is caused by strong electrostatic interactions between these highly charged objects. The SAXS diagram of $\mathbf{D_{Si}[tpy]}$ (1 mM in DMSO-d_6) in the presence of 1 equiv of $[Fe(H_2O)_6](ClO_4)_2$ displays additional oscillations that correspond to distance larger than the POMs dimension. The theoretical SAXS patterns of the energy-minimized structures of the molecular triangle $[(\mathbf{D_{Si}[tpy]})_3{\cdot}\mathbf{Fe_3}]$ (in which Zn have been replaced by Fe atoms) have been computed using the program CRYSOL (Figure 3b)[66] without any adjustment of free parameters. If we ignore the decrease in intensity caused by the electrostatic interactions, we notice that the intensity at small q values (ca. 0.03 Å^{-1}), which is proportional to the molar mass of the molecular system in case of monodisperse assemblies,[67] is perfectly reproduced, which supports the triangular structure. A slight difference is however observed in the first oscillation, suggesting that the POM−POM distance in the calculated molecular triangle is underestimated possibly due to the bent shape of the organic linker. This also may suggest the formation of larger cyclic oligomeric species such as a molecular square. To this end, the structure of a potential molecular square was also investigated by DFT calculations, using the same methodology as previously described for the molecular triangle. The coordinates of the resulting optimized structure (featuring pairs of POMs on opposite vertices oriented in the same direction) are given in Table S3 and published online.[58] When computing the SAXS patterns of the energy-minimized structure of the molecular square $[(\mathbf{D_{Si}[tpy]})_4{\cdot}\mathbf{Fe_4}]$ (Figure S6), the first oscillation is better reproduced than for the molecular triangle $[(\mathbf{D_{Si}[tpy]})_3{\cdot}\mathbf{Fe_3}]$. However, the calculated intensity either at small wave vectors (ca. 0.03 Å^{-1}) and large wave vectors (ca. 0.4−0.6 Å^{-1}) does not satisfactoryly fit with the experimental data, so that the molecular square was not further considered.

Aggregation of the Supramolecular Triangles. Upon the addition of any polar solvent (CD_3CN, acetone-d_6, D_2O, ...) to a solution of $[(\mathbf{D_{Si}[tpy]})_3{\cdot}\mathbf{Fe_3}]$ in DMSO-d_6, ill-defined ^{1}H signals appear in the aromatic region while the solution remains homogeneous and displays its characteristic purple coloration attesting the persistence of the Fe(II) bis-terpyridine complexes. NMR DOSY experiments in such solvent mixtures failed to obtain ^{1}H signals in the aromatic region. This is characteristic of colloidal systems displaying low T_2 relaxation.[68] The ^{1}H NMR spectrum of a solution of $\mathbf{D_{Si}[tpy]}$ (1 mM) in the presence of 1 equiv of $[Fe(H_2O)_6](ClO_4)_2$ in a mixture of DMSO-d_6/CD_3CN (1:1, v/v) shows both signals of the discrete molecular triangle $[(\mathbf{D_{Si}[tpy]})_3{\cdot}\mathbf{Fe_3}]$ and those ill-defined of the new supramolecular assemblies. However, in a DMSO-d_6/CD_3CN (1:4, v/v) mixture, only ^{1}H NMR signals of the new species are observed (Figure 4a). Interestingly, upon

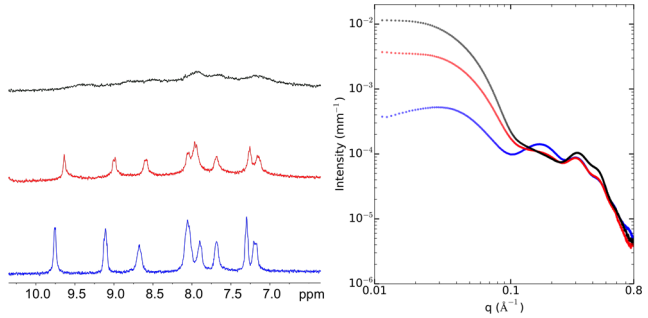

Figure 4. ^{1}H NMR spectra (300 MHz, left) and SAXS curves (right) of solutions of $\mathbf{D_{Si}[tpy]}$ (1 mM) in the presence of 1 equiv of $[Fe(H_2O)_6](ClO_4)_2$ in DMSO-d_6 (blue), DMSO-d_6/CD_3CN (1/1) (red), and DMSO-d_6/CD_3CN (1/4) (black).

removal of CD_3CN from DMSO-d_6/CD_3CN mixtures containing $\mathbf{D_{Si}[tpy]}$ in the presence of 1 equiv of $[Fe(H_2O)_6](ClO_4)_2$, the ^{1}H NMR signals of the molecular triangle $[(\mathbf{D_{Si}[tpy]})_3{\cdot}\mathbf{Fe_3}]$ are quantitatively restored, attesting the reversibility of the process.

SAXS experiments were performed with the same DMSO-d_6/CD_3CN mixtures containing $\mathbf{D_{Si}[tpy]}$ (1 mM) and 1 equiv of $[Fe(H_2O)_6](ClO_4)_2$. The signal intensity in the low-q region significantly increases with the molar fraction of CD_3CN suggesting the formation of aggregated species. The signal intensity in the low-q region (ca. 0.03 Å^{-1}) is enhanced by a factor of ca. 6 and ca. 18 in DMSO-d_6/CD_3CN (1:1, v/v) and (1:4, v/v) mixtures, respectively (Figure 4b). Hence, an 18-fold increase between the molecular triangle in DMSO-d_6 signal and

DOI: 10.1021/jacs.6b00972
J. Am. Chem. Soc. 2016, 138, 5093−5099

that of the assembly in a DMSO-d_6/CD_3CN (1:4, v/v) mixture is consistent with an aggregate composed of ca. 54 POMs. From the Guinier regime of SAXS curve[69] in the DMSO-d_6/CD_3CN (1:4, v/v) mixture, we can also extract a radius of gyration of the aggregates r_g = 3.9 nm. Interestingly the oscillations at $q > 10^{-1}$ nm^{-1} characteristic of the molecular triangle $[(\mathbf{D_{Si}[tpy]})_3{\cdot}\mathbf{Fe_3}]$, albeit attenuated, are still present in the SAXS patterns in all DMSO-d_6/CD_3CN mixtures. This indicates that the new supramolecular assembly is formed by the aggregation of the molecular triangle and remains nanostructured, the molecular triangle acting as a secondary building unit of the overall supramolecular assembly. We previously described the crystal structure of a silyl-pyrene terminated derivative of a Dawson-type POM as a tetrabutyl ammonium salt.[70] In the crystal packing, the volume occupied by a POM-based hybrid is 4520 $Å^3$. A sphere with r = 3.9 nm would thus contain ca. 55 POMs that is amazingly very close to the 54 POMs per assembly obtained by SAXS. This suggests that the nanoparticle-like assemblies have a maximum compactness.

In the previous bis-pyridine POM-based supramolecular triangle, the binding sites were coordinated to a neutral metal linker, i.e., $Pd^{II}Cl_2$. This system did not self-assemble into a more complex species when changing the composition of the solvent. In the present case, the discrete cyclic coordination oligomer $[(\mathbf{D_{Si}[tpy]})_3{\cdot}\mathbf{Fe_3}]$ presents a regular alternation of anionic (POMs) and cationic (metal) moieties, which is likely to favor aggregation through electrostatic interactions. The aggregation processes are dictated by the nature of the solvent and particularly its dissociating ability. In a strongly dissociating solvent such as DMSO, the electrostatic interaction between the cyclic oligomers is weak so that the discrete molecular triangles are observed. In contrast, in a lower dissociating solvent such as acetonitrile, the metallomacrocycles act as secondary building units and further self-assemble in small dense nanoparticles whose anionic nature provide stability in solution.[33]

Transmission electron microscopy (TEM) of the dispersed supramolecular assembly was performed after the deposition of few drops of a solution of $\mathbf{D_{Si}[tpy]}$ (25 μM) in the presence of 1 equiv of $[Fe(H_2O)_6](ClO_4)_2$ in acetonitrile on a Cu grid covered with an amorphous carbon film. Electron micrographs at high magnification unambiguously show the presence of monodisperse small nanoparticle-like assemblies with 7.5 ± 1 nm diameters (Figure 5), in full agreement with the radius of gyration obtained by SAXS. Inspection of the particles allows the observation of nanometer size POMs that appear more contrasted than the covalent organic tether and the TBA counterions due to their important electron density.

The chemical analysis by EDS shows the presence of the main elements constituting the particles (i.e., W, O, C, Si, and Fe, Figure S7). No Cl atom is present in the particle, in agreement with the absence of perchlorate anion. In contrast, electron micrographs of dispersed $\mathbf{D_{Si}[tpy]}$ in acetonitrile do not show any organization of the POMs(Figure S8).

Important numbers of self-assemblies of POMs lead to the formation of large hollow structures such as vesicles or blackberry-like structures (usually in the 30−100 nm scale).[10] Similarly, POM-based paddle-wheel macroclusters[31] formed by metal-directed self-assembly of a hexamolybdate functionalized with a carboxylic acid unit coordinated to copper ions also assemble into such large hollow-like structure in suitable solvents. We herein report a second type of a hierarchical

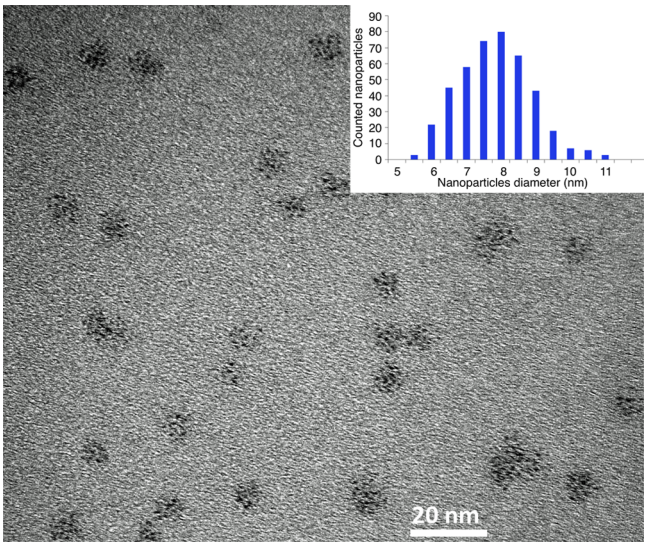

Figure 5. TEM micrographs and size histogram (inset) of the nanoparticle-like assemblies $[(\mathbf{D_{Si}[tpy]})_3{\cdot}\mathbf{Fe_3}]_n$.

organization from POM-based building blocks to discrete supramolecular assemblies and then to larger nanoscales structures. In the present case, the POM-based supramolecular triangles self-assemble into unprecedented dense monodisperse nanoparticles (Scheme 2). The difference between these two types of assemblies probably arises from the presence of the electrostatic interactions between the primary supramolecular assemblies due to the presence of negatively charged POMs and cationic metal linkers within their structure.

While the size of the reported blackberry structures vary according to the composition of the solvent, in our system ^{1}H NMR shows that in DMSO-d_6/CD_3CN mixtures, the discrete molecular triangle is in equilibrium with the aggregated assembly. This suggests that the solvent composition impacts more likely the equilibrium between both supramolecular forms rather than the size of the multiscale assembled system. According to TEM experiments, the supramolecular particles are isotropic. The control over the shape of the hierarchical self-assemblies remains a very attractive challenge. This could be obtained by controlling additional intermolecular interactions between the primary supramolecular assemblies.[71] Cooperation of different noncovalent interactions, including hydrophobic, electrostatic, and hydrogen-bonding ones, is the key to forming ordered extended assemblies with emergent properties.[3,72−74] To this end, the choice of the counterions associated with the POM is an important lever in the control of the aggregation process. According to their hydrophilic/hydrophobic character, the counterions should provide segregation[75] in appropriate solvent mixtures and thus allow the control of the nanostructure arrangement as a result of the overall intermolecular interactions at work.

■ CONCLUSION

We have synthesized a new ditopic POM-based building-block bearing remote terpyridine units and studied its self-assembly behavior in the presence of a linking metal cation. In a strongly dissociating solvent (DMSO), the hybrid spontaneously assembles into a discrete supramolecular assembly, which was characterized by NMR and SAXS experiments. In the presence of less dissociating solvent (MeCN), the primary supramolecular structure self-assembles into dense monodisperse

DOI: 10.1021/jacs.6b00972
J. Am. Chem. Soc. 2016, 138, 5093−5099

Scheme 2. Schematic Representation of the Formation of the Nanosized Aggregates by Hierarchical Self-Assembly of D_{Si}[tpy] upon Complexation with Fe^{2+}

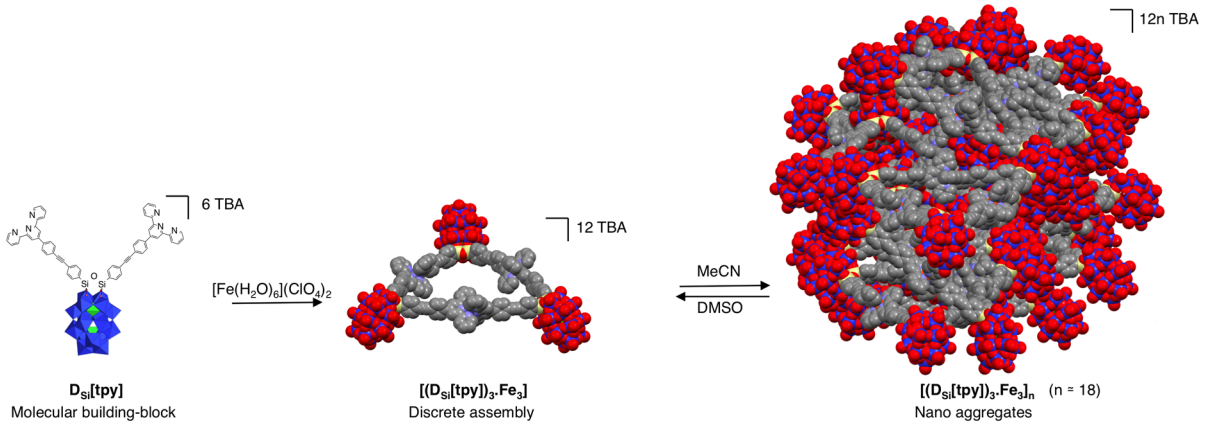

nanoparticles, characterized through SAXS and TEM, and forms a hierarchical organization, this process being fully reversible. Further studies will focus on the control the shape and size of the overall assembly by modification of the primary POM-based building blocks and their associated counterions.

■ ASSOCIATED CONTENT

Supporting Information

The Supporting Information is available free of charge on the ACS Publications website at DOI: 10.1021/jacs.6b00972. A dataset collection is available at http://dx.doi.org/10.19061/iochem-bd-1-5.

Descriptions of the experimental and calculation details (PDF)

■ AUTHOR INFORMATION

Corresponding Author

*guillaume.izzet@upmc.fr

Notes

The authors declare no competing financial interest.

■ ACKNOWLEDGMENTS

Dr. Laurent Bouteiller is greatly acknowledged for fruitful discussion. We acknowledge SOLEIL for provision of synchrotron radiation facilities and we would like to thank Javiez Pérez and for assistance in using beamline SWING. We also thank Dr. Sandra Alves for performing the MS analysis of the POM-based building block **D_{Si}[tpy]**. The Severo Ochoa Excellence Accreditation (SEV-2013-0319) and the COST Action CM1203 "Polyoxometalate Chemistry for Molecular Nanoscience (PoCheMoN)" are gratefully acknowledged. This work was supported by the French National Research Agency (EXPAND, ANR-14-CE08-0002). S.A.S. and C.B. also wish to thank the Marie Curie/COFUND funding scheme (291787-ICIQ-IPMP), the Spanish Ministerio de Economia y Competitividad (MINECO) (CTQ2014-52824-R), the Generalitat de Catalunya (project 2014SGR409), and the ICIQ Foundation.

■ REFERENCES

(1) Whitesides, G. M.; Kriebel, J. K.; Mayers, B. T. *Self-Assembly and Nanostructured Materials*; Springer: Berlin, 2005.
(2) Faul, C. F. J. *Acc. Chem. Res.* **2014**, *47*, 3428.
(3) Rest, C.; Kandanelli, R.; Fernandez, G. *Chem. Soc. Rev.* **2015**, *44*, 2573.
(4) Chen, L. J.; Ren, Y. Y.; Wu, N. W.; Sun, B.; Ma, J. Q.; Zhang, L.; Tan, H. W.; Liu, M. H.; Li, X. P.; Yang, H. B. *J. Am. Chem. Soc.* **2015**, *137*, 11725.
(5) Inokuma, Y.; Kawano, M.; Fujita, M. *Nat. Chem.* **2011**, *3*, 349.
(6) Song, Y. F.; Tsunashima, R. *Chem. Soc. Rev.* **2012**, *41*, 7384.
(7) Proust, A.; Matt, B.; Villanneau, R.; Guillemot, G.; Gouzerh, P.; Izzet, G. *Chem. Soc. Rev.* **2012**, *41*, 7605.
(8) Miras, H. N.; Yan, J.; Long, D. L.; Cronin, L. *Chem. Soc. Rev.* **2012**, *41*, 7403.
(9) Polarz, S.; Landsmann, S.; Klaiber, A. *Angew. Chem., Int. Ed.* **2014**, *53*, 946.
(10) Yin, P. C.; Li, D.; Liu, T. B. *Chem. Soc. Rev.* **2012**, *41*, 7368.
(11) Giner-Casares, J. J.; Brezesinski, G.; Mohwald, H.; Landsmann, S.; Polarz, S. *J. Phys. Chem. Lett.* **2012**, *3*, 322.
(12) Noro, S.; Tsunashima, R.; Kamiya, Y.; Uemura, K.; Kita, H.; Cronin, L.; Akutagawa, T.; Nakamura, T. *Angew. Chem., Int. Ed.* **2009**, *48*, 8703.
(13) Polarz, S.; Smarsly, B.; Antonietti, M. *ChemPhysChem* **2001**, *2*, 457.
(14) Li, W.; Bu, W. F.; Li, H. L.; Wu, L. X.; Li, M. *Chem. Commun.* **2005**, 3785.
(15) Scullion, R. A.; Surman, A. J.; Xu, F.; Mathieson, J. S.; Long, D. L.; Haso, F.; Liu, T. B.; Cronin, L. *Angew. Chem., Int. Ed.* **2014**, *53*, 10032.
(16) Pradeep, C. P.; Misdrahi, M. F.; Li, F. Y.; Zhang, J.; Xu, L.; Long, D. L.; Liu, T. B.; Cronin, L. *Angew. Chem., Int. Ed.* **2009**, *48*, 8309.
(17) Yin, P. C.; Wu, P. F.; Xiao, Z. C.; Li, D.; Bitterlich, E.; Zhang, J.; Cheng, P.; Vezenov, D. V.; Liu, T. B.; Wei, Y. G. *Angew. Chem., Int. Ed.* **2011**, *50*, 2521.
(18) Landsmann, S.; Wessig, M.; Schmid, M.; Colfen, H.; Polarz, S. *Angew. Chem., Int. Ed.* **2012**, *51*, 5995.
(19) Jallet, V.; Guillemot, G.; Lai, J.; Bauduin, P.; Nardello-Rataj, V.; Proust, A. *Chem. Commun.* **2014**, *50*, 6610.
(20) Yan, Y.; Wang, H. B.; Li, B.; Hou, G. F.; Yin, Z. D.; Wu, L. X.; Yam, V. W. W. *Angew. Chem., Int. Ed.* **2010**, *49*, 9233.
(21) Chakrabarty, R.; Mukherjee, P. S.; Stang, P. J. *Chem. Rev.* **2011**, *111*, 6810.
(22) Yamada, T.; Otsubo, K.; Makiura, R.; Kitagawa, H. *Chem. Soc. Rev.* **2013**, *42*, 6655.
(23) He, W. W.; Li, S. L.; Zang, H. Y.; Yang, G. S.; Zhang, S. R.; Su, Z. M.; Lan, Y. Q. *Coord. Chem. Rev.* **2014**, *279*, 141.
(24) Du, D. Y.; Qin, J. S.; Li, S. L.; Su, Z. M.; Lan, Y. Q. *Chem. Soc. Rev.* **2014**, *43*, 4615.
(25) Santoni, M. P.; Hanan, G. S.; Hasenknopf, B. *Coord. Chem. Rev.* **2014**, *281*, 64.

DOI: 10.1021/jacs.6b00972
J. Am. Chem. Soc. 2016, 138, 5093−5099

(26) Santoni, M. P.; Pal, A. K.; Hanan, G. S.; Tang, M. C.; Venne, K.; Furtos, A.; Menard-Tremblay, P.; Malveau, C.; Hasenknopf, B. *Chem. Commun.* **2012**, *48*, 200.
(27) Han, J. W.; Hardcastle, K. I.; Hill, C. L. *Eur. J. Inorg. Chem.* **2006**, *2006*, 2598.
(28) Han, J. W.; Hill, C. L. *J. Am. Chem. Soc.* **2007**, *129*, 15094.
(29) Kang, J.; Xu, B. B.; Peng, Z. H.; Zhu, X. D.; Wei, Y. G.; Powell, D. R. *Angew. Chem., Int. Ed.* **2005**, *44*, 6902.
(30) Izzet, G.; Macdonell, A.; Rinfray, C.; Piot, M.; Renaudineau, S.; Derat, E.; Abécassis, B.; Afonso, C.; Proust, A. *Chem. - Eur. J.* **2015**, *21*, 19010.
(31) Zhu, Y.; Yin, P. C.; Xiao, F. P.; Li, D.; Bitterlich, E.; Xiao, Z. C.; Zhang, J.; Hao, J.; Liu, T. B.; Wang, Y.; Wei, Y. G. *J. Am. Chem. Soc.* **2013**, *135*, 17155.
(32) Dong, B.; Sakurai, T.; Honsho, Y.; Seki, S.; Maeda, H. *J. Am. Chem. Soc.* **2013**, *135*, 1284.
(33) Gröhn, F. *Soft Matter* **2010**, *6*, 4296.
(34) Willerich, I.; Gröhn, F. *Angew. Chem., Int. Ed.* **2010**, *49*, 8104.
(35) Klosterman, J. K.; Yamauchi, Y.; Fujita, M. *Chem. Soc. Rev.* **2009**, *38*, 1714.
(36) Acronyms used for the hybrid POMs: D refers to the Dawson-type anion, Si as subscript relates to the primary functionalization and the term in brackets corresponds to the remote organic moieties.
(37) Duffort, V.; Thouvenot, R.; Afonso, C.; Izzet, G.; Proust, A. *Chem. Commun.* **2009**, 6062.
(38) Morris, K. F.; Johnson, C. S. *J. Am. Chem. Soc.* **1993**, *115*, 4291.
(39) Morris, K. F.; Johnson, C. S. *J. Am. Chem. Soc.* **1992**, *114*, 3139.
(40) Schaeffer, G.; Fuhr, O.; Fenske, D.; Lehn, J. M. *Chem. - Eur. J.* **2014**, *20*, 179.
(41) Fonseca Guerra, C.; Snijders, J. G.; te Velde, G.; Baerends, E. J. *Theor. Chem. Acc.* **1998**, *99*, 391.
(42) te Velde, G.; Bickelhaupt, F. M.; Baerends, E. J.; Fonseca Guerra, C.; van Gisbergen, S. J. A.; Snijders, J. G.; Ziegler, T. *J. Comput. Chem.* **2001**, *22*, 931.
(43) Becke, A. D. *Phys. Rev. A: At., Mol., Opt. Phys.* **1988**, *38*, 3098.
(44) Perdew, J. P. *Phys. Rev. B: Condens. Matter Mater. Phys.* **1986**, *33*, 8822.
(45) Perdew, J. P. *Phys. Rev. B: Condens. Matter Mater. Phys.* **1986**, *34*, 7406.
(46) Grimme, S.; Antony, J.; Ehrlich, S.; Krieg, H. *J. Chem. Phys.* **2010**, *132*, 154104.
(47) Grimme, S.; Ehrlich, S.; Goerigk, L. *J. Comput. Chem.* **2011**, *32*, 1456.
(48) Johnson, E. R.; Becke, A. D. *J. Chem. Phys.* **2006**, *124*, 174104.
(49) van Lenthe, E.; Baerends, E. J.; Snijders, J. G. *J. Chem. Phys.* **1993**, *99*, 4597.
(50) van Lenthe, E.; Baerends, E. J.; Snijders, J. G. *J. Chem. Phys.* **1994**, *101*, 9783.
(51) Becke, A. D. *J. Chem. Phys.* **1988**, *88*, 2547.
(52) Franchini, M.; Philipsen, P. H. T.; Visscher, L. *J. Comput. Chem.* **2013**, *34*, 1819.
(53) Wang, Y. A.; Yam, C. Y.; Chen, Y. K.; Chen, G. *J. Chem. Phys.* **2011**, *134*, 241103.
(54) Klamt, A. *J. Phys. Chem.* **1995**, *99*, 2224.
(55) Klamt, A.; Jonas, V. *J. Chem. Phys.* **1996**, *105*, 9972.
(56) Klamt, A.; Schüürmann, G. *J. Chem. Soc., Perkin Trans. 2* **1993**, 799.
(57) Klamt, A.; Jonas, V.; Bürger, T.; Lohrenz, J. C. W. *J. Phys. Chem. A* **1998**, *102*, 5074.
(58) http://dx.doi.org/10.19061/iochem-bd-1-5.
(59) Vreven, T.; Byun, K. S.; Komáromi, I.; Dapprich, S.; Montgomery, J. A.; Morokuma, K.; Frisch, M. J. *J. Chem. Theory Comput.* **2006**, *2*, 815.
(60) Frisch, M. J.; Trucks, G. W.; Schlegel, H. B.; Scuseria, G. E.; Robb, M. A.; Cheeseman, J. R.; Scalmani, G.; Barone, V.; Mennucci, B.; Petersson, G. A.; Nakatsuji, H.; Caricato, M.; Li, X.; Hratchian, H. P.; Izmaylov, A. F.; Bloino, J.; Zheng, G.; Sonnenberg, J. L.; Hada, M.; Ehara, M.; Toyota, K.; Fukuda, R.; Hasegawa, J.; Ishida, M.; Nakajima, T.; Honda, Y.; Kitao, O.; Nakai, H.; Vreven, T.; Montgomery, J. A., Jr.; Peralta, J. E.; Ogliaro, F.; Bearpark, M. J.; Heyd, J.; Brothers, E. N.; Kudin, K. N.; Staroverov, V. N.; Kobayashi, R.; Normand, J.; Raghavachari, K.; Rendell, A. P.; Burant, J. C.; Iyengar, S. S.; Tomasi, J.; Cossi, M.; Rega, N.; Millam, N. J.; Klene, M.; Knox, J. E.; Cross, J. B.; Bakken, V.; Adamo, C.; Jaramillo, J.; Gomperts, R.; Stratmann, R. E.; Yazyev, O.; Austin, A. J.; Cammi, R.; Pomelli, C.; Ochterski, J. W.; Martin, R. L.; Morokuma, K.; Zakrzewski, V. G.; Voth, G. A.; Salvador, P.; Dannenberg, J. J.; Dapprich, S.; Daniels, A. D.; Farkas, Ö.; Foresman, J. B.; Ortiz, J. V.; Cioslowski, J.; Fox, D. J.; *Gaussian09*, Rev. D.01 ed.; Gaussian, Inc.: Wallingford, CT, 2009.
(61) Wasielewski, M. R. *Acc. Chem. Res.* **2009**, *42*, 1910.
(62) Sprafke, J. K.; Kondratuk, D. V.; Wykes, M.; Thompson, A. L.; Hoffmann, M.; Drevinskas, R.; Chen, W. H.; Yong, C. K.; Karnbratt, J.; Bullock, J. E.; Malfois, M.; Wasielewski, M. R.; Albinsson, B.; Herz, L. M.; Zigmantas, D.; Beljonne, D.; Anderson, H. L. *J. Am. Chem. Soc.* **2011**, *133*, 17262.
(63) Hou, Y.; Zakharov, L. N.; Nyman, M. *J. Am. Chem. Soc.* **2013**, *135*, 16651.
(64) Yin, P. C.; Zhang, J.; Li, T.; Zuo, X. B.; Hao, J.; Warner, A. M.; Chattopadhyay, S.; Shibata, T.; Wei, Y. G.; Liu, T. B. *J. Am. Chem. Soc.* **2013**, *135*, 4529.
(65) Wu, Y. L.; Shi, R. F.; Wu, Y. L.; Holcroft, J. M.; Liu, Z. C.; Frasconi, M.; Wasielewski, M. R.; Li, H.; Stoddart, J. F. *J. Am. Chem. Soc.* **2015**, *137*, 4111.
(66) Svergun, D.; Barberato, C.; Koch, M. H. J. *J. Appl. Crystallogr.* **1995**, *28*, 768.
(67) Svergun, D. I.; Koch, M. H. J. *Rep. Prog. Phys.* **2003**, *66*, 1735.
(68) Osborne, E. A.; Jarrett, B. R.; Tu, C. Q.; Louie, A. Y. *J. Am. Chem. Soc.* **2010**, *132*, 5934.
(69) Als-Nielsen, J.; McMorrow, D. *Elements of Modern X-ray Physics*; Wiley: New York, 2001.
(70) Matt, B.; Renaudineau, S.; Chamoreau, L. M.; Afonso, C.; Izzet, G.; Proust, A. *J. Org. Chem.* **2011**, *76*, 3107.
(71) Whitesides, G. M.; Grzybowski, B. *Science* **2002**, *295*, 2418.
(72) Luisi, P. *Found. Chem.* **2002**, *4*, 183.
(73) Hunter, C. A.; Anderson, H. L. *Angew. Chem., Int. Ed.* **2009**, *48*, 7488.
(74) Bruns, C. J.; Fujita, D.; Hoshino, M.; Sato, S.; Stoddart, J. F.; Fujita, M. *J. Am. Chem. Soc.* **2014**, *136*, 12027.
(75) Kato, T. *Science* **2002**, *295*, 2414.

DOI: 10.1021/jacs.6b00972
J. Am. Chem. Soc. 2016, 138, 5093−5099